Case Studies in Construction Materials 20 (2024) e03002

Contents lists available at ScienceDirect

Case Studies in Construction Materials

journal homepage: www.elsevier.com/locate/cscm

Slag-based stabilization/solidification of hazardous arsenic-bearing tailings as cemented paste backfill: Strength and arsenic immobilization assessment

Haiqiang Jiang [a,b], Jingru Zheng [a], You Fu [a], Zhuoran Wang [a], Erol Yilmaz [c,*], Liang Cui [d,*]

[a] Key Laboratory of Ministry of Education on Safe Mining of Deep Metal Mines, Northeastern University, Shenyang 110819, China
[b] State Key Laboratory for Fine Exploration and Intelligent Development of Coal Resources, China University of Mining and Technology, Xuzhou 221116, China
[c] Department of Civil Engineering, Geotechnical Division, Recep Tayyip Erdogan University, Fener, Rize TR53100, Turkiye
[d] Department of Civil Engineering, Lakehead University, Thunder Bay, Ontario, P7B 5E1 Canada

ARTICLE INFO

Keywords:
Arsenic-bearing tailings
Alkali-activated slag
Backfill
Arsenic immobilization
Strength

ABSTRACT

The widespread occurrence of toxic arsenic in sulfidic and non-ferrous waste tailings hinders its disposal as cement paste backfill (CPB). Alkali activated slag (AAS) has recently begun to be practiced as an alternative to normal Portland cement (OPC). Nevertheless, technical information on arsenic immobilization and mechanical characteristics of arsenic-rich AAS-CPB is rather few. The impacts of activator nature, cure temperature and arsenic content on strength and arsenic immobilization of AAS-CPB explored. Despite AAS-CPB having greater strength, OPC-CPB consistently has a stronger (1.7–21.1% higher) ability to immobilize arsenic. The optimum silica modulus for maximal strength and arsenic immobilization capability depends on curing time. Strength at3 days is enhanced by higher activator doses, whereas strength at later ages ($\geq$ 28 days) is decreased. At all curing ages, the lowest arsenic immobilization capacity is produced by medium activator concentration (0.35). Irrespective of cement type, strength increases as curing temperature rose, however OPC-CPB's strength is more responsive to temperature changes than AAS-CPB's. At room temperature (20°C), OPC-CPB has a higher (6.0–21.1% greater) arsenic immobilization efficiency (AIE) than AAS-CPB, but the opposite is true at lower (5°C) and higher (35°C) temperatures (i.e., 5.4–12.0% and 4.4–12.0% lower at 5 and 35°C respectively). Early on, the influence of arsenic content on strength is not immediately apparent, but it tends to become more obvious with longer curing times. As a role of cement type and elapsed time, high arsenic contents cause a rise or a decrease in AIE. Notably, there is no apparent connection between UCS and AIE. Electrical conductivity and moisture content can be steadily employed to portray the hydration progression of both arsenic-free and arsenic-containing CPB.

1. Introduction

Regularly characterized by high solubility and significant toxicity at low concentrations, arsenic (As) is highly toxic [1–3]. Statistics

* Corresponding authors.
E-mail addresses: erol.yilmaz@erdogan.edu.tr (E. Yilmaz), liang.cui@lakeheadu.ca (L. Cui).

https://doi.org/10.1016/j.cscm.2024.e03002
Received 25 November 2023; Received in revised form 16 January 2024; Accepted 20 February 2024
Available online 21 February 2024

show that China has ~71 of arsenic reserves worldwide [4], and over 30 Mt of arsenic waste are created each year from mining processing of Cu/Pb/Zn ores [5]. Arsenic typically occurs in concentrations of hundreds or even thousands of parts per million (ppm) in sulfide-bearing and non-ferrous metal mineral deposits [6]. Moreover, arsenic-containing by-products, such as arsenic trioxide, can be made during the refining of gold [7,8]. Arsenic can oxidize to trivalent or pentavalent forms in neutral or acidic environments, and it can then be liberated as a variety of soluble species [9,10]. Arsenic can leak into the soil or ground water as a result of the arsenic-bearing tailings that are deposited on the ground surface being washed by precipitation or surface water. This can lead to cross-regional pollution transfer, ecosystem deterioration, and related human health hazards [11]. There have been reports of arsenic pollution in gold mining regions in Brazil, Mexico, Canada, and Spain [12,13].

Cement-based paste backfill (CPB) is a mine filling technique currently applied for effective and sustainable disposal of process wastes currently produced in huge amounts every year [14–16]. Together, tailings, hydraulic binder, and water make up CPB masses [17–19]. Hydraulic binder contributes to advancement of CPB's strength features [20–22]. Arsenic-bearing process tailings were effectively stabilized/solidified using normal Portland cement (OPC) centered binders [7,23,24]. Li et al. [4] concluded that during the initial 3 days arsenic was immobilized by physically encapsulated Ca-As species, while As-ettringite dominated the key arsenic immobilization process. However, Bothe and Brown [25] found that precipitation of Ca-As should be regarded as the key source of arsenic production. Similarly, researches from [26] and [27] argued that arsenic reacts with calcium in alkaline pore water in the anions formation of $HAsO_4^{2-}$ and AsO_4^{3-} to form calcium arsenate or calcium arsenite precipitation. The arsenic immobilization capability has been shown to be strongly influenced by the type of binder [28,29]. Coussy et al. [24] found that in contrast to CPB made of OPC-based binder, CPB with fly ash based binder emitted a higher amount of arsenic. Bull and Fall [23] experimentally investigated the difference between CPB specimens made of OPC (OPC-CPB) and OPC/slag blend (50%/50%) in terms of arsenic immobilisation ability at various cure heats (5–35°C). Results showed that at upper cure heats, more arsenic escaped from OPC-CPB specimens, whereas under identical curing conditions, less arsenic escaped sample made of OPC/Slag blend. Hamberg et al. [7] emphasized that slurry's water saturation is a major feature governing As leaching rate of the CPB system.

Traditional OPC-based binders are, however, costly and produce a lot of greenhouse gases during production [30,31]. Meanwhile, CPB made of OPC-based binders is susceptible to sulphate attack, leading to the deterioration of mechanical properties and heavy metal immobilization. It has been proven that as compared to OPC-CPB. CPB made of alkali-activated slag (AAS-CPB) exhibits superior properties such as higher early strength [32–34], better flowability [35–38], lower heat of hydration [39], and more desirable durability [39]. However, technical information on the arsenic immobilization and mechanical characteristics of As-rich AAS-CPB is quite limited. There still exist numerous unanswered questions. For instance, what are the main factors influencing on the stabilization/solidification of arsenic-bearing tailings? How do the mechanical and immobilization properties change with the curing time? What is the difference in the arsenic-bearing tailings stabilization/solidification between OPC and AAS? As of right now, no research has been done on the important issues described above. This means that if handled unsuitably, AAS-CPB manufactured of As-bearing tailings could pose a threat to the environment. In light of this, the current study seeks:

- to clarify influences of silica modulus (Ms), activator content (AC), cure temperature and arsenic content on compressive strength of AAS-CPB with/without arsenic;
- to estimate the arsenic immobilization characteristics of AAS-CPB made of varying Ms, AC, arsenic content and cured at distinct temperatures;
- to compare the strength and arsenic immobilization features between AAS-CPB and OPC-CPB.

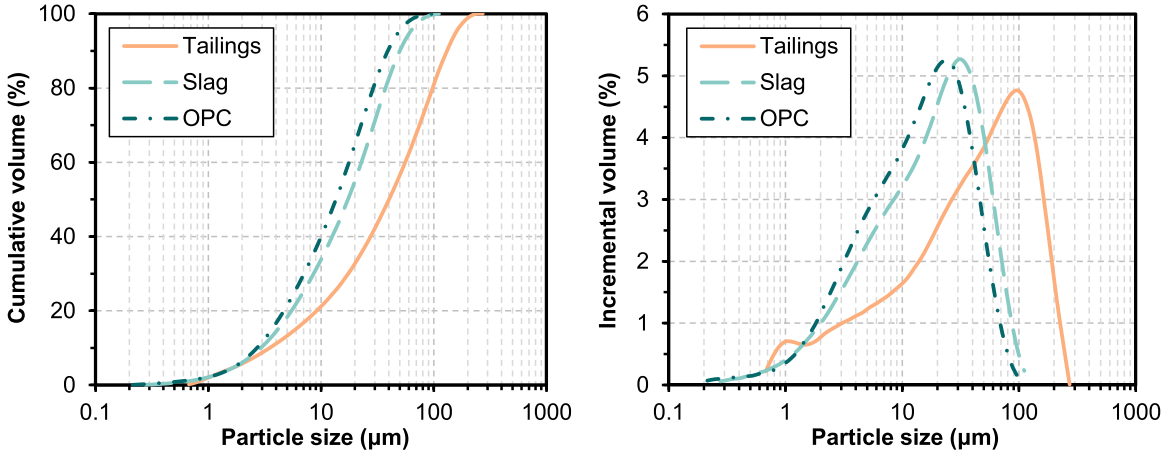

Fig. 1. GSD profiles of ST, slag and OPC.

2. Materials and methods

2.1. Essential components

2.1.1. Arsenious tails

To quantitatively quantify the arsenic solidification characteristics of AAS-CPB, synthetic tailings (ST) with arsenic reagent were utilized to replicate natural tailings that included arsenic. Because ST is mostly inert quartz (>98% by weight), which doesn't contain active or acid-producing materials, Test results are more reliable and less prone to inaccuracy. Fig. 1 demonstrates ST's grain size distribution (GSD) curves, as identified by a laser diffraction grain sizer (Malvern Mastersizer 3000, United Kingdom). It had 32.7% of fine grains below 20 μm. Analytically pure sodium arsenite ($NaAsO_2$) reagent was used to prepare arsenic-bearing tailings. The concentration of arsenic in natural tailings can vary from dozens of ppm to hundreds of thousands of ppm. Considering the range of arsenic concentrations in the majority of natural tailings, arsenic was added until solid concentrations of 3500, 5000, and 6500 ppm, or 0.35, 0.5, and 0.65% of the ST, respectively, are reached.

2.1.2. Binders

AAS and OPC (type 42.5 R in accordance with GB175–2007 as a reference) were utilized as the binding agents. The slag used to prepare AAS was supplied from a local iron and steel plant. The composite alkali activators were synthesized by dissolving granular sodium hydroxide (purity: 99%; SH) into liquid sodium silicate having a Ms of 2.31. OPC is slightly finer-grained than slag. Fig. 1 depicts GSD profiles of slag and OPC while Table 1 summarizes their key physicochemical features.

2.1.3. Water

Mixing water participated in this trial was laboratory tap water (pH: 7.35 and electrical conductivity: 1.93 μs/cm). The specific properties were described in the literature [40].

2.2. Mix proportions

CPB mixtures with various Ms (0.26, 0.3, and 0.34), AC (0.30, 0.35, and 0.40), and arsenic content (0%, 0.35%, 0.5%, and 0.65%) were produced. The solid concentration is set to 77% for all of the mixtures. For AAS-CPBs, the slag proportion is fixed at 5%. It must be noted that the binder fraction in OPC-CPB is the same as in AAS-CPB. The blends' recipes are compiled in Table 2.

2.3. Specimens preparation and curing

The preparation procedures are as follows:

- Dissolve the weighed SH reagent in the mixing water, seal, and cool it to room temperature (about 20°C). The obtained SH solution was then combined in various ratios with water glass to produce alkali activators with desired Ms values;
- ST, slag/OPC, and sodium arsenite reagent was uniformly blended to create a homogeneous solid dry substance;
- Alkali activator was put into solid ingredient and then blended for 300 seconds to manufacture a constant paste mixture;
- Paste mixtures were cast in 30×30×30 mm cubic molds of and sealed with plastic wrap eliminate water evaporation;
- Specimens were left to cure in a room at diverse heats (5−35°C) for up to 56-day.

Table 1
Main physicochemical property of test materials.

Chemical compositions (wt%)	ST	Slag	OPC	Physical properties	ST	Slag	OPC
CaO	-	47.01	62.75	Specific gravity	2.63	2.92	3.18
SiO_2	>99	32.06	20.64	Specific surface (cm^2/g)	232	354	387
Al_2O_3	-	10.53	5.93	-20μm content (%)	32.70	55.01	64.76
MgO	-	5.51	1.22	Basicity coefficient[b]	-	1.22	-
TiO_2	-	0.85	0.75	Hydration modulus[c]	-	2.00	-
Fe_2O_3	-	0.70	3.74	D_{10} (μm)	3.50	2.92	2.71
SO_3	-	1.34	2.37	D_{30} (μm)	17.46	8.60	7.09
K_2O	-	0.54	1.11	D_{50} (μm)	40.1	17.34	13.62
MnO	-	0.23	0.21	D_{60} (μm)	55.97	22.8	17.76
Cr_2O_3	-	-	-	D_{90} (μm)	131.64	50.1	39.27
SrO	-	0.13	0.07	Cu	15.99	7.81	6.55
P_2O_5	-	-	0.12	Cc	1.56	1.11	1.04
LOI[a]	-	1.10	1.10				

b(CaO + MgO) / (SiO2 + Al_2O_3); c(CaO + MgO + Al_2O3) / SiO_2

[a] LOI: Loss-on-ignition.

Table 2
Recipe of the mixtures.

Influencing factor	Binder type	Slag dosage (wt %)	Silica modulus (Ms) (-)	Activator content AC (-)	Arsenic content (wt %)	Curing temperature (°C)
Ms	OPC	-	-	-	0	20
	OPC	-	-	-	0.5	20
	AAS	5	0.26, 0.3, 0.34	0.35	0	20
	AAS	5	0.26, 0.3, 0.34	0.35	0.5	20
AC	OPC	-	-	-	0	20
	OPC	-	-	-	0.5	20
	AAS	5	0.3	0.30, 0.35, 0.40	0	20
	AAS	5	0.3	0.30, 0.35, 0.40	0.5	20
Curing temperature	OPC	-	-	-	0	5, 20, 35
	OPC	-	-	-	0.5	5, 20, 35
	AAS	5	0.3	0.35	0	5, 20, 35
	AAS	5	0.3	0.35	0.5	5, 20, 35
Arsenic content	OPC	-	-	-	0, 0.35, 0.5, 0.65	20
	AAS	5	0.3	0.35	0, 0.35, 0.5, 0.65	20

Note: Ms : $\frac{M_{SiO_2}}{M_{Na_2O}}$; AC : $\frac{M_{activator}}{M_{slag}}$; ($M$: weight;)

2.4. Test procedures

2.4.1. UCS experiment

UCS (uniaxial compressive strength) experiments were realized via a Humboldt HM-5030 loader holding a maximum loading power of 50 kN in keeping with ASTM C39. The triplicate sets of experiments were done by considering 1 mm/minute dislocation ratio. The backfills' end face was flattened and aligned with longitudinal axis.

2.4.2. TCLP experiment

Toxicity characteristic leaching procedure (TCLP), a test practice verified by EPA (environmental protection agency), were used to evaluate CPB's arsenic immobilization efficiency (AIE). Some precise steps are given below:

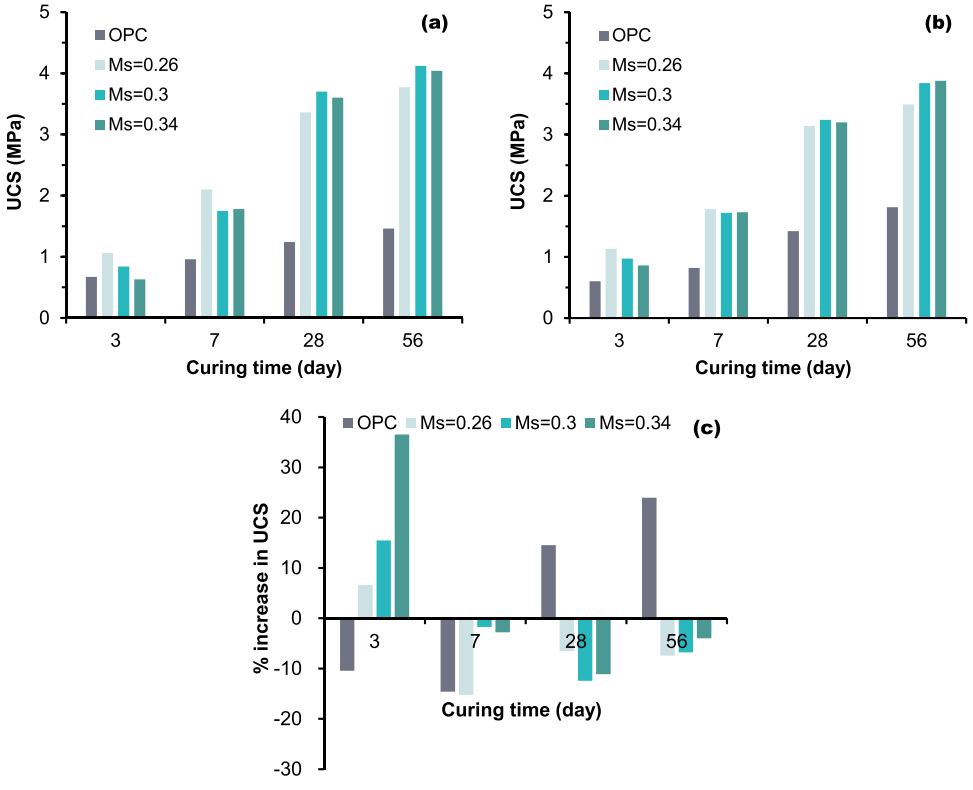

Fig. 2. Ms effect on UCS of (a) arsenic-free CPBs and (b) arsenic-containing CPBs, and (c) arsenic-induced variation in UCS.

- *Preparation of a strong extraction fluid*: 5.7 mL of glacial acetic acid (CH_3CH_2OOH) is diluted to a capacity of 1 L with deionized water. A strong extraction fluid was then acquired with a pH of 2.88.
- *Sample preparation*: After the UCS test, crush the middle of the specimen into small pieces that can fit through a 9.5 mm square-hole sieve to produce cube samples that range in size from 4.5 to 9.5 mm.
- *Rotate and leaching*: Put 75–100 g of sample in the extractor vessel, then slowly add a certain amount of extraction fluid to the extraction vessel in a water/dry rate of 20:1 mL/g. Rotate extraction vessel at 30 rpm retention rapidity for a time duration of 18 hours. During extraction procedure, the ambient temperature is held constant at 23 ± 0.5°C.
- *Collect filtrate and detect concentration:* A 0.45-m filter was used to filter mixture. The arsenic concentration of filtered leachates is identified through the Agilent 5110 SVDV ICP-OES.

2.4.3. Electrical conductivity (EC) and moisture content (MC) measurement

TEROS 12 transducers (Meter Group, United States) were used for clearly monitoring EC and MC values of CPB specimens. To track the constant change in EC and MC over the course of 21 days, the transducers were submerged in a fresh CPB mixture and data was captured every hour.

2.4.4. SEM observation

CPB's microstructure was explored by SIGMA 300 SEM (scanning electron microscopy; Zeiss, Germany) operated at 15 keV, and the microcosmic configuration of arsenic-containing AAS-CPB and OPC-CPBs at different curing ages were obtained.

2.4.5. MIP experiment

The MIP (Mercury intrusion porosimeter) experiments were undertaken by considering the ASTM D4404–18 standard. Before MIP

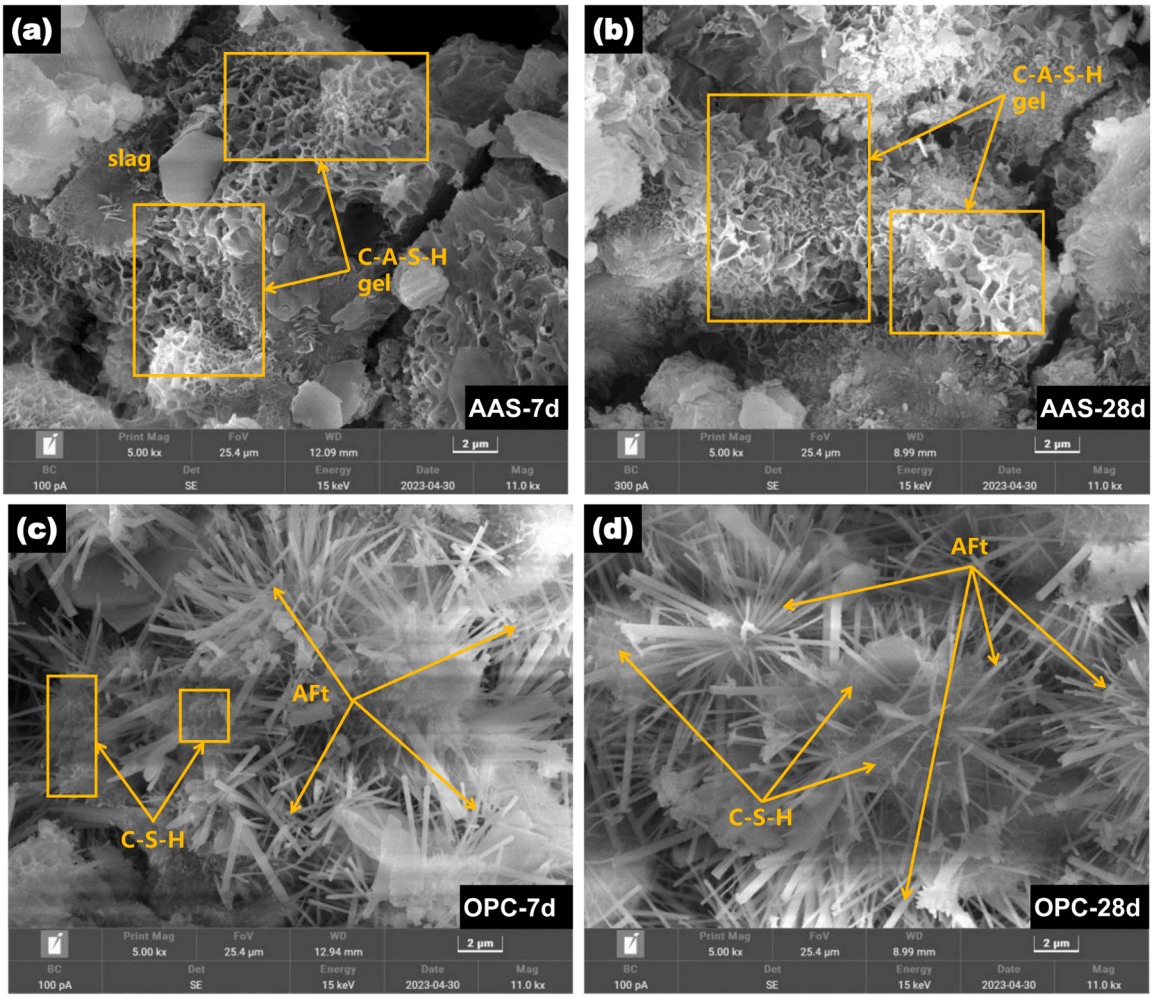

Fig. 3. SEM results of arsenic-containing AAS-CPBs left to cure at (a) 20°C-7d, (b) 20°C-28d and arsenic-containing OPC-CPBs left to cure at (c) 20°C-7d, (d) 20°C-28d.

testing, $1\times1\times1$ cm^3 samples were dehydrated for 1-day at 40°C after being submerged in ethanol for 3-day to stop hydration. An AutoPore IV 9510 porosimeter (Micromeritics, United States) was employed for featuring CPB's pore size/morphology.

3. Results and discussion

3.1. Silica modulus dependency

3.1.1. UCS

Fig. 2(a) depicts impact of Ms on UCS of OPC-CPB and AAS-CPB without arsenic. As time gets advanced, UCS of all CPBs without arsenic rapidly increases, owing to larger amount of hydration products and denser pore structures inside CPB matrixes [41,42]. As expected, AAS-CPB displays higher strength than OPC-CPB at any cure time. This may be clarified via the marked difference in compositions of hydration materials. Ms effect on UCS of arsenic-free AAS-CPB changes over time. At early age (3 days), the UCS declines with increasing Ms (closely linked to low pH, which reduces the intensity of hydration at young ages;[43,44]. At later ages of 28 and 56 days, it is found that medium Ms of 0.3 delivers the greatest AAS-CPB strength. This can be explained by the competing effects that higher Ms reduces the rate of hydration but provides more amount of silica source [45].

Fig. 2(b) demonstrates strength increases of arsenic-containing OPC-CPB and AAS-CPB specimens having different Ms (0.26, 0.3, and 0.34). Similar to arsenic-free samples, arsenic-containing AAS-CPBs exhibit higher strength in tandem with longer curing time. The overall trend of strength for arsenic-containing AAS-CPBs with varied Ms is similar to that of arsenic-free samples, as shown by a comparison of Figs. 2(a) and 2(b). This indicates that arsenic has no obvious impact on strength improvement of AAS-CPBs having variable Ms values. Regardless of Ms and arsenic, AAS-CPBs always have a higher UCS than the OPC-CPBs. Fig. 3 demonstrates the microscopic morphology of arsenic-containing AAS- and OPC-CPB cured for 7- and 28-day. One can clearly detect that the major hydration material of AAS-CPB is C-A-S-H having reticulate configuration, while C-S-H gels and spine bar granular ettringite (AFt) are observed for OPC-CPB. In C-S-H's interlayer region, a rather weak bridge relay between adjacent major layers is provided by calcium ions. The neighboring layers can create stronger covalent bonds as a result of Al ions being pulled into C-S-H configuration [46–48]. In addition, Ca/Si fraction of C-A-S-H from AAS-CPB is too lesser than one of C-S-H from OPC-CPB [40]. These facts help to partly explain why AAS-CPB is substantially stronger than OPC-CPB.

Fig. 2(c) depicts the strength fluctuation brought on by the addition of arsenic. The strength of both OPC-CPBs and AAS-CPBs is clearly influenced by the presence of arsenic. Arsenic increases OPC-CPB's strength at advanced ages (the strength of 28 and 56 days increased by 14.5% and 24.0%, respectively) while weakening it at early ages (respectively 10.5% and 14.6% drop in UCS for 3- and 7-day). This arsenic-induced adverse impact on early-aged fill strength may be clarified by the fact that part of Ca^{2+} ions is consumed via calcium-arsenic precipitates, leading to fewer quantity of Ca^{2+} present for C-S-H formation. A slight drop in concentration of Ca^{2+} will subsequently rise pore fluid's pH due to the solubility product constant, resting on Gibbs free energy concept [49] Previous researches (e.g., [50]) reported that an increase in pH results in more uneven distribution of C-S-H, causing strength features' reduction. Improvement of strength gaining at later curing stages may be explained the fact that the pore solution's pH and alkali concentration affect Ca/Si fraction of C-S-H, and greater pH usually corresponds to lesser Ca/Si fraction of C-S-H [51,52].

Contrarily, in event of AAS-CPB, arsenic residue results in an improvement of the strength during the very first stage (3 days), but a subsequent reduction in strength after that. As explained previously, the addition of arsenic will cause a reduction of Ca^{2+} via calcium-arsenic precipitates, contributing to a rise in pore fluid's pH. A higher pH will accelerate the hydration of AAS binder, thereby causing a promotion in early-aged AAS-CPB strength. However, the consumption of Ca^{2+} in calcium-arsenic precipitates means that indicate sufficient quantity of Ca present to create principal hydration material: C-S-H. Thus a smaller amount of C-S-H gels was shaped [53]. The later-age strength of AAS-CPB is reduced. Arsenic's effects on AAS-CPB's strength are highly susceptible to Ms and curing time. The beneficial effect from arsenic on 3-day strength to AAS-CPB seems to be more significant at higher Ms. Mostly, the addition of arsenic results in strength increases of 6.6%, 15.5%, and 36.5% for AAS-CPB specimens having Ms of 0.26, 0.3, and 0.34, respectively. After 28 days, there seems to be a declining effect of arsenic on the potency of AAS-CPB.

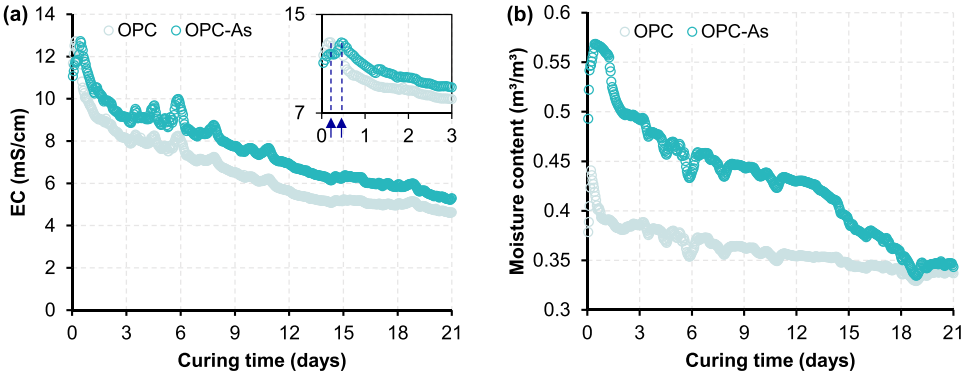

Fig. 4. Evolution of (a) EC and (b) MC of OPC-CPBs with and without arsenic.

Figs. 4(a) and 4(b) depict the evolution of EC and MC of OPC-CPBs with and without arsenic respectively. For arsenic-containing OPC-CPB, the first main peak of the EC curve emerges at roughly 0.5 days, whereas for arsenic-free OPC-CPB, the peak appears at roughly 0.2 days. This fact suggests that arsenic inhibits the hydration of OPC, which may result from the precipitation of Ca-As. Arsenic's inhibitory impact was also supported by the fact that the arsenic-containing OPC-CPB had a higher MC than arsenic-free OPC-CPB. The aforementioned findings explained why OPC-CPB's early age strengths decreased by adding arsenic. As time gets increased, difference in EC and MC between arsenic-free OPC-CPB and arsenic-containing OPC-CPB gradually diminishes. As shown in Fig. 4, the rate of change in MC of the arsenic-containing OPC-CPB was mainly quick compared to that of arsenic-free OPC-CPB. This was along with positive rise in UCS of arsenic-containing OPC-CPB.

Figs. 5(a) and 5(b) show, respectively, the development of EC and MC to AAS-CPBs with and without arsenic. It is evident that the MC of the arsenic-containing AAS-CPB was lower than that of the arsenic-free AAS-CPB within the first 3 days, suggesting that arsenic accelerates the hydration reaction of early age AAS-CPB specimens. This is along with high strength of 3-day strength of arsenic-containing AAS-CPB than that of arsenic-free sample. Afterwards, both EC and MC of arsenic-containing AAS-CPB decrease at a lesser proportion than one of arsenic-free specimen. After that, the arsenic-containing AAS-CPB decreases in EC and MC at a slower rate than the arsenic-free sample. This recommends that the occurrence of arsenic hinders 3-day cured AAS-CPB's hydration. This is along with outcomes of strength beyond 3 days presented in Fig. 2.

3.1.2. Arsenic immobilization

The time-variant AIE of OPC-CPBs and AAS-CPBs with varying Ms is shown in Fig. 6. It is evident that Ms and curing time are dependent variables on the AIE irrespective of the type of binder. As opposed to a greater range of AIE from 76.2% to 83.0% for AAS-CPBs, the AIE of OPC-CPBs gradually varies from 84.3% to 85.9%. This surprise outcome shows that OPC-CPB outperforms AAS-CPB in terms of arsenic immobilization capacity, despite the latter having higher UCS. This notable disparity in AIE could be clarified by distinct contrast in configuration of raw product and hydration materials between OPC and AAS. First of all, amount of Ca^{2+} ions in the pore solution dissolved from Ca-rich OPC is much higher than that from AAS (Ca is only contained in slag). This means that more amount of arsenic will be immobilized by calcium-arsenic precipitates in OPC-CPB than AAS-CPB. Conversely, OPC's hydration also produce appreciable quantity of AFt. Due to its needle bar granular structure, AFt has more active sites for arsenic adsorption than C-S-H or C-A-S-H gels. Additionally, SO_4^{2-} of AFt on external surface of $[Al(OH)_6]^{3-}$ allows for replacement of SO_4^{2-} by O_2-containing anions having related constructions and bond lengths. Thus, AsO_4^{3-} can be fixed in AFt structure by the substitution of isomorphic [54,55]. In case of C-A-S-H or C-S-H, arsenic is most anticipated to be fixed by adsorption or connect with Si-O at the terminus of the silicate chain, but its stability is poorer than that through the substitution of isomorphic. The above analysis explains the greater AIE of OPC-CPB than AAS-CPB. This indicates that physical adsorption is not the determining mechanism for As solidification, considering the much higher strength and denser microstructure (see Fig. 9) of AAS-CPB. Bull and Fall [23] and Coussy et al. [24] found that AIE of CPB made of OPC/Slag blend (50%/50%) was pointedly lesser than one of OPC-CPB.

A Ms of 0.3 is discovered to produce the lowest AIE at all curing ages from 3 days to 56 days. All specimens' AIEs develop in a similar manner, with a gradually enhancement at early age tracked by a minor drop thereafter. Sole difference is that turning point for AAS-CPB happens sooner than for OPC-CPB (at 7 days vs 28 days). However, this slight reduction in AIE for both AAS-CPB or OPC-CPB are beyond the scope of the study.

Comparing the results of UCS (Fig. 2(b)) to AIE (Fig. 6(a)) reveals that at all curing ages AAS-CPBs show higher strength than OPC-CPB whilst the reverse is true in the case of AIE. Meanwhile, for all samples, the strength continuously grew with the extend of curing time, whist the corresponding AIE shows a slight decrease. Additionally, it appears that Ms' impact on the UCS differs from that on the AIE. To better illustrate the link between UCS and AIE, the UCS values are plotted against the corresponding AIE values (Fig. 6(b)). The scattered points suggest that there is no clear link between UCS and AIE.

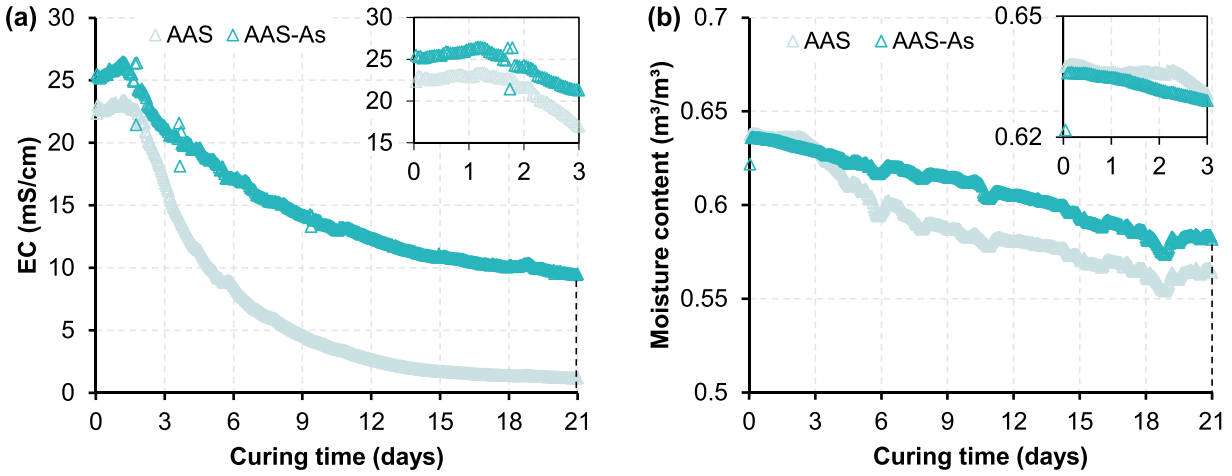

Fig. 5. Progress of (a) EC and (b) MC of AAS-CPB specimens with and without arsenic (Ms: 0.3).

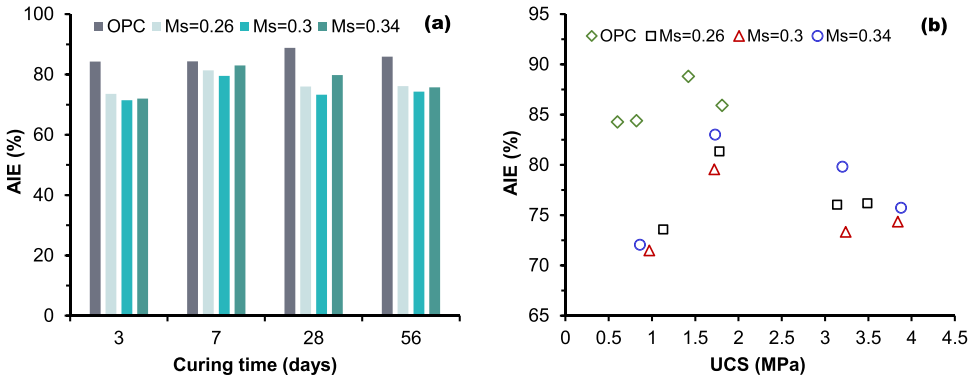

Fig. 6. (a) AIE and (b) AIE versus UCS of OPC-CPBs and AAS-CPBs with various Ms.

3.2. Activator concentration dependency

3.2.1. UCS

Fig. 7 demonstrates UCS features of OPC-CPB and AAS-CPBs produced of different AC (0.30, 0.35, and 0.40) and with or without As up to 56 days. For all AAS-CPBs, the Ms of the activator was fixed to 0.3. Each specimen that contains arsenic has a 0.5% arsenic concentration. Fig. 7(a) shows that all samples' UCS grows with extended curing age. The constant hydration of slag grains results in extra hydration products, creating a denser and stiffer microstructure [56–58]. Compared to arsenic-free OPC-CPB, all arsenic-free AAS-CPBs, regardless of AC levels, steadily display greater strength. Increasing AC causes UCS of AAS-CPB without arsenic to rise for first 3 days of curing but to decline after that point. This is due to the fact that at younger ages, rising AC is linked to a higher concentration of OH-, which will speed up cement hydration. However, excessively intense and fast precipitation of AAS's hydration materials can form a protective shell, preventing the dissolution of unreacted slag at later ages [59–61].

Fig. 7(b) demonstrates the change of UCS for arsenic-containing OPO- and AAS-CPB over time. Trend in UCS development of arsenic-containing AAS-CPB is similar to that of arsenic-free AAS-CPB, i.e., UCS increases with increased AC at 3 days and exhibits a clearly opposing pattern at 28 and 56 days. This implies that the effect of AC on the UCS is virtually independent of arsenic. Regardless

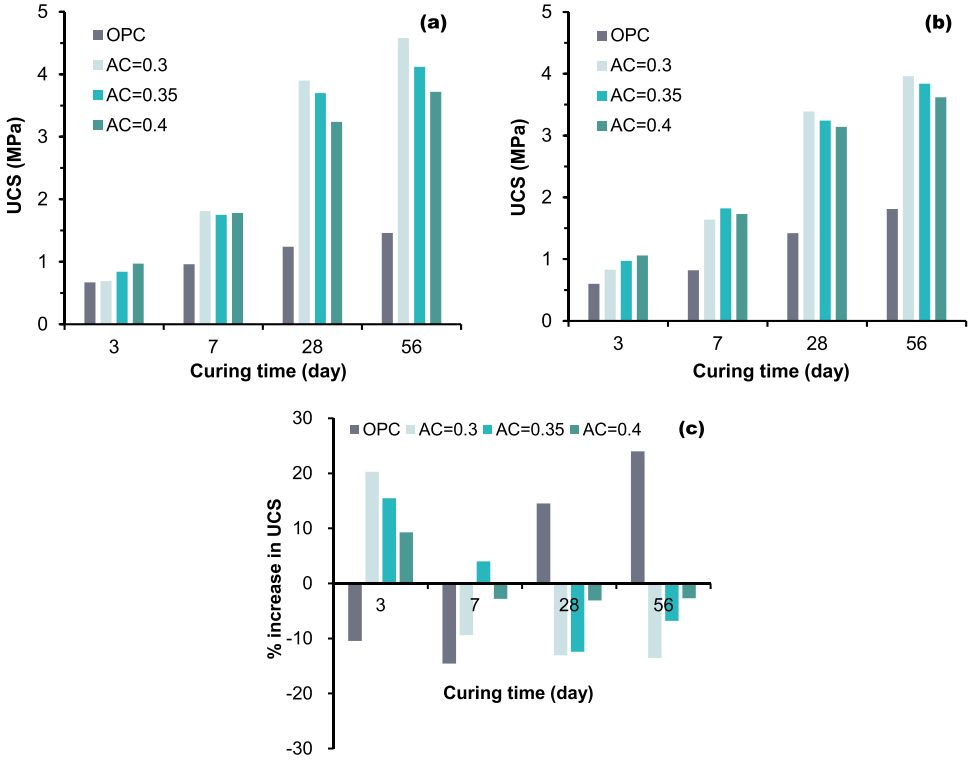

Fig. 7. AC effect on strength acquisition of (a) arsenic-free CPBs and (b) arsenic-containing CPBs, and (c) arsenic-induced variation in UCS.

of whether they contain arsenic, AAS-CPB has greater UCS than OPC-CPB. This difference in UCS between AAS- and OPC-CPB starts to widen with longer curing time.

The arsenic-induced variation in UCS of OPC-CPB and AAS-CPB is illustrated in Fig. 7(c). OPC-CPB and AAS-CPBs react to the presence of arsenic in radically different ways. For OPC-CPB, arsenic lowers the UCS at 3 and 7 days, but raises it beyond 7 days. For AAS-CPB, the inclusion of arsenic results in a 9.3–20.3% increase in strength at 3 days, however as the curing time passes, this preferred effect gradually changes into a negative impact. Arsenic's impact on the UCS appears to vary depending on AC. The magnitude of the impact, whether positive or negative, decreases with increasing AC.

3.2.2. Arsenic immobilization

Fig. 8(a) displays the AIE for both AAS and OPC based CPB specimens with varying activator concentrations. The AIE of OPC-CPB specimens at each age is clearly superior to that of AAS-CPB specimens. The greatest AIE of AAS-CPB specimens is only 79.69%, 81.08%, 78.67%, and 78.97%, respectively, while the AIE of OPC-CPB specimens reaches 84.28%, 84.39%, 88.80%, and 85.91% at 3-, 7-, 28-, and 56-day, respectively. One can deduce that OPC has a significantly larger ability for bonding arsenic than AAS given the higher strength of AAS-CPB than OPC-CPB. All AAS-CPB specimens have an arsenic immobilization capability that increases with extended curing times up to 7 days, but steadily declines after that until it reaches a plateau after 28 days. Overall, among all AAS-CPB specimens with varied AC at all curing ages, AAS-CPB with a medium degree of AC (0.3) has the lowest AIE value. Similar to the case of AAS-CPB with different Ms, the plotting of AIE versus UCS in Fig. 8(b) indicates that there is no clear correlation between UCS and AIE for AAS-CPB made of various AC.

Fig. 9(a) and (b) displays the cumulative/incremental pore volumes of arsenic-containing AAS-CPBs and OPC-CPBs cured for 7 and 28 days. It is clear that arsenic-containing AAS-CPB specimens have less cumulative pore volume than OPC-CPB ones. The AIE of AAS-CPB, which has a finer microstructure, is, however, less effective than OPC-CPB. This suggests that physical encapsulation is not the decisive factor in arsenic immobilization. It is surprised to found that the cumulative pore volume of AAS-CPB increases dramatically from 7 days to 28 days. This finding coincidentally supports the decline in AIE over the same time period. Usually, pore size distribution can be categorized as 4 portions by considering the effects on development of strength and permeability: fine capillary/gel pores (< 50 nm), intermediate (50−100 nm) and large (100 nm−10 μm) capillary pores, and macro pores (> 10 μm). Fig. 9(c) shows the proportion of pore volume associated with distinct pore size portions. Regardless of binder type, 28-day cured specimens have a decreased volume of pores larger than 100 nm compared to 7-day cured specimens, which can be clarified by the creation of further accumulated hydration materials. For OPC-CPB and AAS-CPB, the volume of both gel/fine and middle capillary pores increase with the curing age, while the volume of large capillary and macro pores display the opposite trend. These outcomes recommend that existing As increases micropore (< 100 nm) number as curing time elapses, which may be the cause of the decrease in AIE with time for both AAS-CPB and OPC-CPB.

3.3. Curing temperature dependency

3.3.1. UCS

Figs. 10(a) and 10(b) shows advances in the strength property of AAS-CPBs or OPC-CPB specimens subjected to an ageing heat of up to 35°C with or without arsenic. The slag dosage, Ms, and AC of AAS-CPB specimens are kept constant at 5%, 0.3 and 0.35, respectively. Each specimen containing arsenic maintains a 0.5% solid concentration and arsenic content. Each arsenic-containing specimen's solid concentration and arsenic content remain at 77% and 0.5%, respectively.

Fig. 10(a) illustrates the strength growth trend for arsenic-free AAS-CPB or OPC-CPB exposed to ageing heat to up to 35°C. It is obvious that UCS development tendency of AAS-CPB specimens could be affected by heat and time of ageing. UCS of AAS-CPB specimens cured in an ageing heat of 35°C consistently outperforms specimens cured at lower temperatures during the initial 28-day curing. This is since higher temperature quickens slag particles' early hydration, causing production of greater hydration materials and, as a result, enhanced mechanical strength [62–64]. But as time passes, this circumstance is changing. The rate of UCS growth

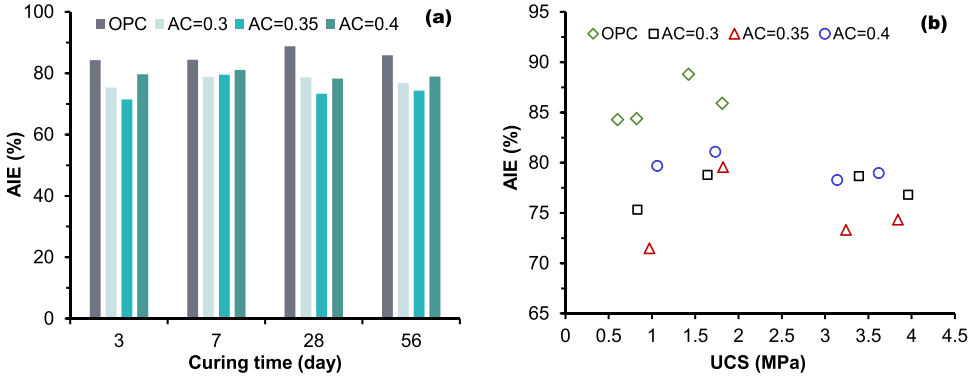

Fig. 8. (a) AIE and (b) AIE versus UCS of both OPC-CPB and AAS-CPBs with various AC.

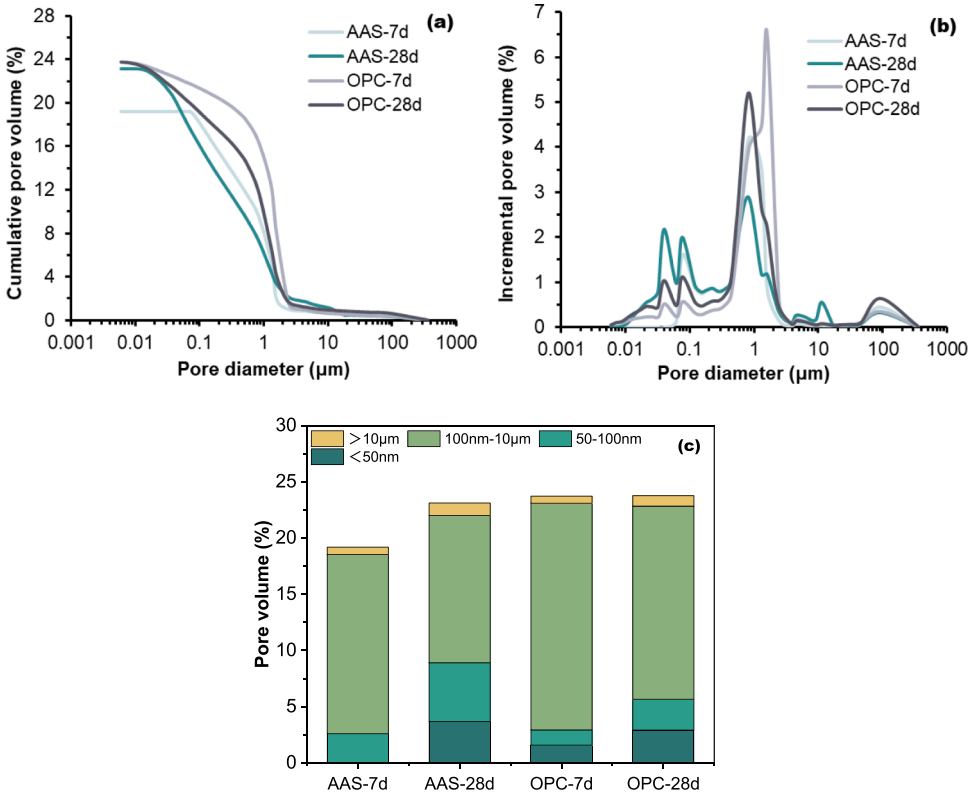

Fig. 9. (a) Cumulative intrusion; (b) incremental intrusion; and (c) pore volume of arsenic-containing AAS-CPB and OPC-CPB.

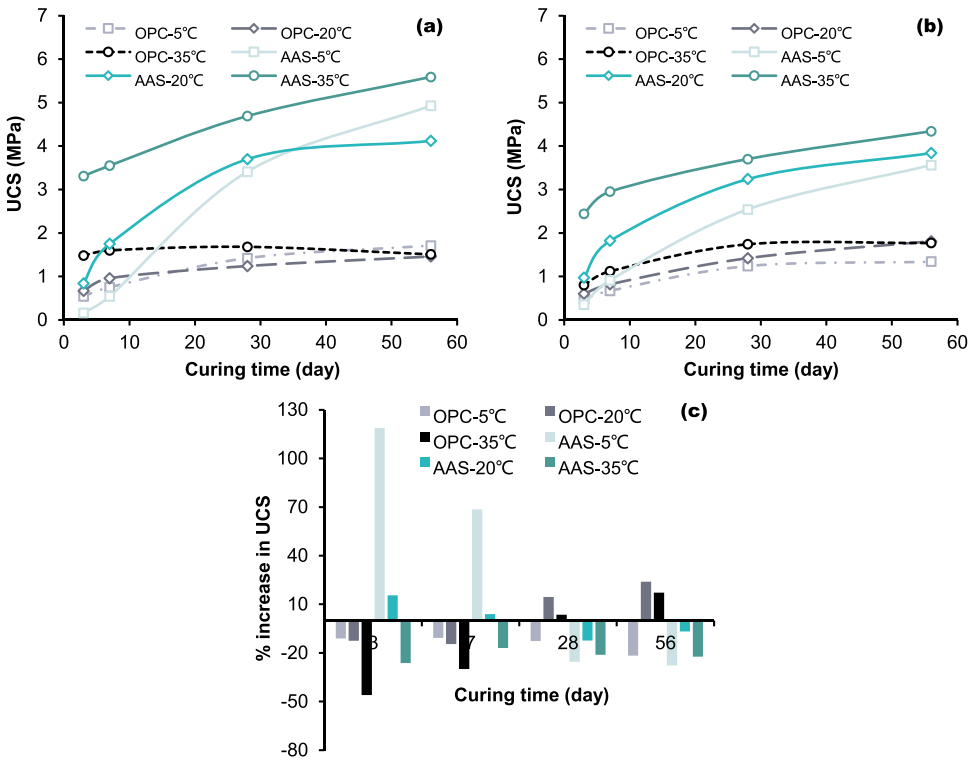

Fig. 10. Curing heat effect on strength of (a) arsenic-free CPBs and (b) arsenic-containing CPBs, and (c) arsenic-induced changes in strength.

after 7-day decreases as the curing temperature rises. As an illustration, UCS of AAS-CPB specimens left to cure at an ageing heat of 5°C and 35°C increases by 813% and 57%, respectively, over the course of 7–56 days. The strength of the AAS-5°C sample finally outperformed the AAS-20°C sample at 56 days due to a discrepancy in the strength growth rate at various temperatures. As explained above, the cause is that higher curing temperatures cause hydration products to prematurely precipitate on the surface of unreacted

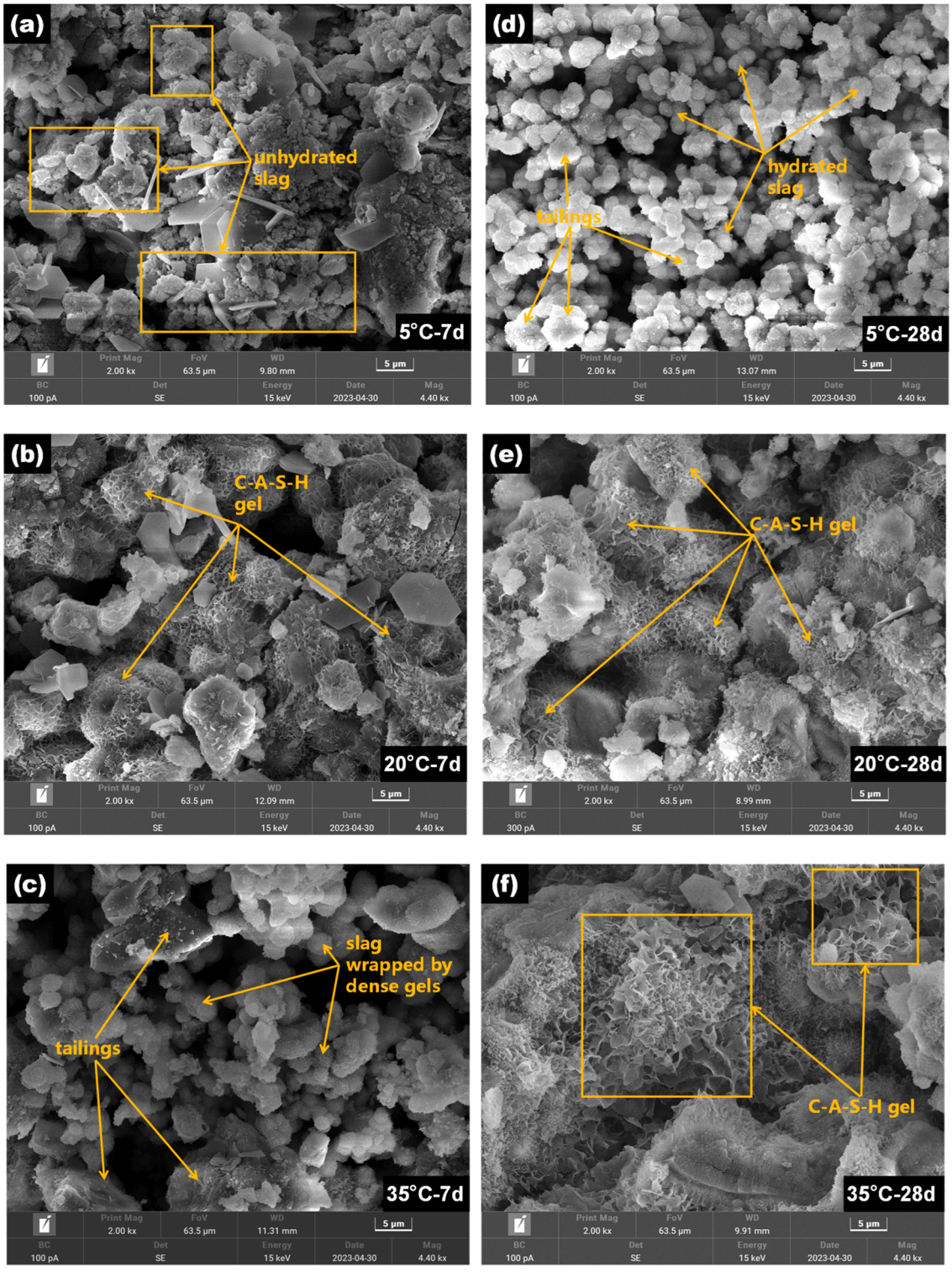

Fig. 11. SEM results of arsenic-containing AAS-CPBs left to cure at (a) 5°C-7d, (b) 20°C-7d, (c) 35°C-7d, (d) 5°C-28d, (e) 20°C-28d, (f) 35°C-28d.

slag particles, functioning as an obstacle to stop the unreacted slag from approaching into interaction by the alkali activator (will be evidenced by the SEM results below). As a result, the strength growth rate decreases at higher temperatures. Although its early-age strength is somewhat restricted, AAS-CPB cured at a lower temperature has a softer hydration that is on the side of uniform distribution of C-S-H gels.

Fig. 10(b) indicates ageing heat effect on UCS of arsenic-containing CPB specimens as a role of time. Arsenic-containing AAS-CPB exposed to different ageing heats has the same order of strength growth rate as arsenic-free samples. Arsenic-containing AAS-CPBs' strength at all ages follows the order of AAS-35°C > AAS-20°C > AAS-5°C as opposed to arsenic-free samples. Fig. 11 displays the SEM results of AAS-CPB that was cured at various temperatures for 7- and 28-day. Regardless of ageing heat, microstructure of arsenic-containing AAS-CPBs grows denser over time. It is obvious that higher curing temperatures cause slag particles to react to a greater extent, which increases the quantity of hydration materials formed and, ultimately, increases UCS. It is worth noting that at high temperature of 35 °C the hydration products fail to diffuse in time and tightly wrap unreacted slag particles.

The results shown in Fig. 10(a) and (b) show that, with the exception of specimens left to cure at 5°C for up to 7-day, UCS of arsenic and arsenic-free AAS-CPBs is upper than one of OPC-CPBs left to cure at identical ageing heat. Additionally, it is clear that OPC-CPBs at identical ageing heat develop UCS more slowly than AAS-CPB specimens over a course of curing age, regardless of the presence of arsenic.

For instance, the strength of arsenic-free AAS-CPB specimens left to cure at an ageing heat of 5°C and 35°C increases by 2981% and 69%, respectively, but the comparable values for OPC-CPBs are 216%, 117%, and 2%. Besides, UCS of OPC-CPB specimens, in contrast to AAS-CPB, is steady or even declines after 28 days, as anticipated. High ageing heat can accelerate creation of micro-cracks in OPC-based backfills [65,66].

Fig. 10(c) depicts the arsenic-induced changes in strength to AAS-CPB/OPC-CPB specimens cured at different ageing heats. The impact of arsenic on the strength depends on cement type, ageing heat, and curing time. The existence of arsenic extensively increases strength at young ages (7 days) but diminishes 28- and 56-day strengths of AAS-CPBs at low (5°C) and medium (20°C) temperatures. Arsenic, however, seems to prevent hydration and, therefore, UCS growth of AAS-CPBs when cured at a high temperature (35°C). OPC-CPB specimens are in a different situation than AAS-CPB specimens. Early-aged (3–7 day) OPC-CPB strength left to cure at 20°C and 35°C is inhibited by existing arsenic, and this inhibitory action intensifies with increasing curing temperature. However, in the later period (28 and 56 days), the presence of arsenic encourages the development of strength of OPC-CPB. At 5°C, arsenic consistently prevents the development of UCS in OPC-CPB specimens. These results suggest that the arsenic solidification mechanisms of AAS- and OPC-CPB specimens differ significantly.

3.3.2. 3.3.2 Arsenic immobilization

Fig. 12(a) shows the results of AIE to both AAS-CPB or OPC-CPB cured with distinctive curing temperatures. With the raised ageing heat, AIE of all specimens left to cure for 3- and 7-day rose. Indeed, a higher curing temperature will accelerate the dissolution of slag particles, producing more amount of Ca^{2+} and AFt and thus allowing higher immobilization of arsenic. However, Bull and Fall [11] reported that the arsenic fixing capacity of mature OPC-CPB (90 days old) decreased as cure temperature climbed from 2°C to 35°C. While ageing at 20°C gives maximum AIE for OPC-CPB specimens, it produces the lowest AIE for AAS-CPB specimens cured for 28-and 56-day. AAS-CPB specimens left to cure at 5°C displayed higher AIE as the age increased, whist the AIE at 20°C and 35°C first grows, then after the drops, finally approaches to stability. On the whole, the AIE of all OPC-CPB specimens tends to rise, then somewhat decline. As previous proved by the MIP results, this declines in the AIE at later ages may be clarified by coarseness of CPB microstructure induced by adding As. At medium temperature, the AIE of OPC-CPB is upper than one of AAS-CPB, but reverse is true at both 5°C and 35°C (except AAS-CPB specimens left to cure at 5°C for 3-day). As expected, no obvious relationship between UCS and AIE was observed for both OPC-CPB and AAS-CPB treated at diverse temperatures (Fig. 12(b)).

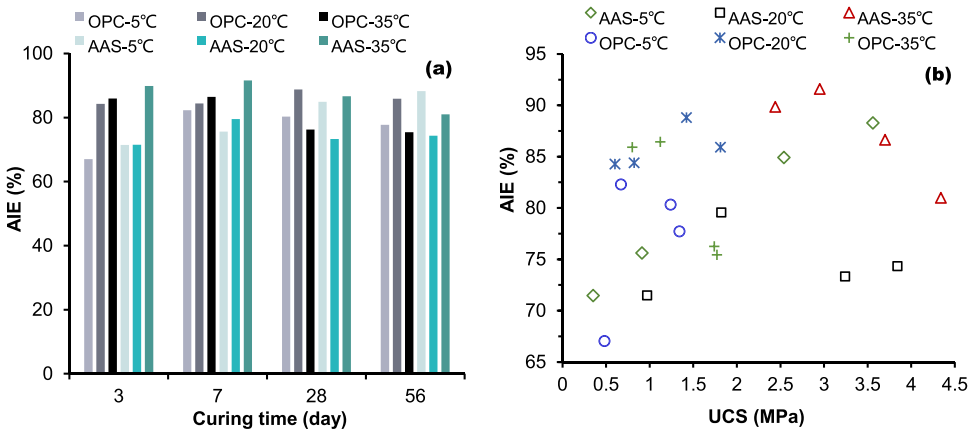

Fig. 12. (a) AIE and (b) AIE versus UCS of AAS-CPB/OPC-CPB at different ageing heats.

3.4. Arsenic content dependency

3.4.1. UCS

To examine the influence of arsenic content. the solid concentration, slag dosage, Ms, and AC of AAS-CPB specimens are consistent and are 77%, 5%, 0.3, and 0.35, respectively. OPC-CPB specimens have the same solid concentration and binder content as the AAS-CPB specimens. Fig. 13(a) indicates UCS performance for AAS-CPB/OPC-CPB specimens with diverse arsenic contents. As anticipated, UCS performance of all AAS-CPBs constantly increases with longer curing ages. 7-day UCS of As-containing AAS-CPB specimens appears to be superior to that of arsenic-free specimens, and follows the following descending order: AAS-0.35% > AAS-0.65% > AAS-0.5% > AAS-0%. AAS-CPB specimens with higher levels of arsenic, however, exhibit a slower rate of strength buildup over time. This results in the 56-day strength of arsenic-free AAS-CPB specimens being greater than that of arsenic-containing specimens, with the 56-day strength degrading with increasing arsenic level.

Similar to AAS-CPB, OPC-CPB's strength and development are likewise influenced by arsenic, but the outcome is almost the opposite. Arsenic has a passive effect early on and a favorable effect later on for the strength of OPC-CPB, as is readily apparent. AAS-CPB specimens are stronger than OPC-CPB at the same arsenic level, especially at later ages.

Fig. 13(b) shows the strength change caused by the addition of arsenic to AAS-CPB and OPC-CPB specimens. At all ages, low content (0.35%) of arsenic increases the strength of AAS-CPB specimens, however this enhancement steadily declines over the course of the curing process, reaching nearly nothing at 56 days. However, medium and high contents (0.5% and 0.65%) of arsenic cause an increase in strength gaining of 3- and 7-day cured AAS-CPB specimens but a reduction at later ages. It appears that there is no clear relationship between arsenic content and magnitude of effect. Arsenic addition's boosting or inhibitory effect on the durability of AAS-CPB specimens increasingly deteriorates with extended curing time. The presence of arsenic in OPC-CPB reduces the strength in early stages (3- and 7-day) but increases UCS at later ages.

3.4.2. Arsenic immobilization

Fig. 14(a) displays the AIE of AAS- and OPC-CPB specimens with varying amounts of arsenic. The AIE of 3- and 7-day cured AAS-CPB specimens drops slightly as amount of arsenic increases, whilst specimens containing medium (0.5%) arsenic has the lowest AIE at 28 and 56 days. The former may be clarified by the fact that AAS-CPBs with diverse contents of arsenic contain the same amount of slag, i.e., the amount of Ca available for arsenic immobilization is constant. As time elapses, AIE of AAS-CPB specimens rises first and then decreases slightly, finally maintaining a stable value. This evolutive trend in AIE is consistent with those of CPBs made of different Ms, AC and cured at various temperatures. The findings suggested that, other from arsenic fixing features at early age, long-term immobilization performance should also be carefully studied before disposal arsenic-containing tailings into subsurface. Comparative investigation demonstrates that at identical arsenic dosage and cure time, AIE of OPC-CPB specimens is superior to that of AAS-CPB specimens. As expected, no obvious relationship is detected for AIE and UCS of CPB with various contents of arsenic (Fig. 14(b)).

4. Conclusions

In laboratory investigation, influences of activator nature, ageing heat and arsenic content on UCS gaining and arsenic immobilization of arsenic-free and arsenic-containing CPB specimens were explored. Besides, CPB's pore structure, which addresses hydration products and microstructural changes, was also analyzed. The following findings were obtained from all these studies.

- The strength of all CPBs rises with longer curing times regardless of the kind of binder and the amount of arsenic used. OPC-CPB consistently has a higher capacity to immobilize arsenic at room temperature, despite AAS-CPB having a denser microstructure and better strength. Notably, there is no discernible link between UCS and AIE for OPC-CPB and AAS-CPB. Arsenic impact on hydration of OPC-CPB and AAS-CPB can be roughly described by using EC and MC.
- The optimum Ms for AAS-CPB's maximum strength and capacity to immobilize arsenic relies on the curing time. Arsenic strengthens AAS-CPB at early age (3 days), weakens it later, and almost has the reverse effect on OPC-CPB. The beneficial effect from arsenic on 3-day strength to AAS-CPB seems to be more pronounced at higher Ms. After 28 days, arsenic's impact on AAS-CPB's efficacy appears to be waning.
- Strength at younger ages is increased by larger activator dosages regardless of the presence of arsenic, whereas strength at older ages was diminished. The effect of arsenic on the UCS seems to differ depending on AC. With rising AC, the extent of the impact—whether favorable or negative—decreases. The medium AC produces the lowest arsenic immobilization capacity at all curing ages. The decrease in AIE of AAS-CPB from 7 to 28 days, may be attributed to the coarsening of micro pores.
- The strength of both arsenic-containing OPC-CPB and AAS-CPB rises as cure temperature rose, however OPC-CPB's strength is more responsive to temperature changes than AAS-CPB's. OPC-CPB has a higher arsenic immobilization efficiency (AIE) than AAS-CPB at ambient temperature (20°C), but at lower (5°C) and higher (35°C), the opposite is true.
- The effect of arsenic content on strength is not apparent at early ages, but it tended to become more apparent with extended curing times. AAS-CPB having high arsenic concentration show a slower proportion of strength development over time. Arsenic can rise or fall UCS of AAS-CPB specimens, based on arsenic concentration and age. High arsenic concentration causes a rise or drop in AIE considering cement type and age.

Some main factors influencing the compressive strength and arsenic immobilization of AAS-CPB was explored in this study. The funding should be conductive to the safe disposal of hazardous arsenic-bearing tailings as cemented paste backfill. However, the

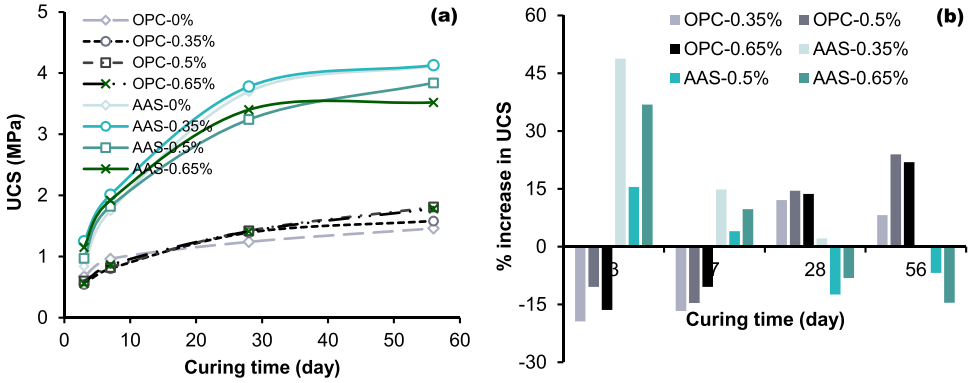

Fig. 13. Strength development (a) and variation of OPC-CPB and AAS-CPB with various contents of arsenic.

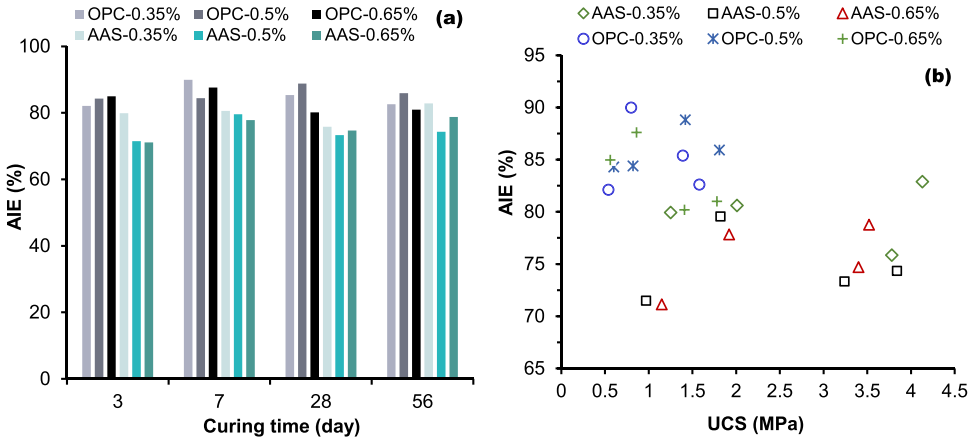

Fig. 14. (a) AIE and (b) AIE versus strength of AAS-CPB and OPC-CPB with several contents of arsenic.

highest arsenic content used in the experiment is only 6500 ppm, which is much lower than (312,000 ppm) that found in natural tailings. It is possible that when arsenic concentration exceeds the threshold value, its effect on the mechanical properties may be completely different. Thus, it is crucial to explore mechanical and immobilization features of AAS-CPB having higher level of arsenic. CPB's immobilization ability and strength gaining is also a result of interaction of many factors such as pore fluid chemistry and pH, type and amount of hydration product, and microstructure. Thus, further investigation of the mechanisms responsible for the variation of strength and leachability is needed. Moreover, the arsenic immobilization of AAS binder is found inferior to OPC. Thus, enhancing arsenic immobilization of AAS-CPB by chemical/mineral modification will be the future work of writers.

CRediT authorship contribution statement

You Fu: Investigation, Data curation. **Jingru Zheng:** Writing – original draft, Methodology, Investigation. **Erol Yilmaz:** Writing – review & editing, Validation, Investigation. **Zhuoran Wang:** Writing – original draft, Validation. **Liang Cui:** Writing – review & editing, Formal analysis, Conceptualization. **Haiqiang Jiang:** Writing – review & editing, Supervision, Conceptualization.

Declaration of Competing Interest

The authors declare that they have no known competing financial interests or personal relationships that could have appeared to influence the work reported in this paper.

Data availability

No data was used for the research described in the article.

Acknowledgements

China's National Key R@D Program (grant number 2023YFC2907203) and Research Fund of State Key Laboratory for Fine Exploration and Intelligent Development of Coal Resources, CUMT (grant no: SKLCRSM23KF005) provided generous financial support to undertake the present investigation.

References

[1] J.E. Langsch, M. Costa, L. Moore, P. Morais, A. Bellezza, S. Falcão, New technology for arsenic removal from mining effluents, J. Mater. Res. Technol. 1 (3) (2012) 178–181, https://doi.org/10.1016/S2238-7854(12)70030-3.
[2] E. Iakovleva, P. Maydannik, T.V. Ivanova, M. Sillanpää, W.Z. Tang, E. Mäkilä, J. Salonen, A. Gubal, A.A. Ganeev, K. Kamwilaisak, S. Wang, Modified and unmodified low-cost iron-containing solid wastes as adsorbents for efficient removal of As(III) and As(V) from mine water, J. Clean. Prod. 133 (2016) 1095–1104, https://doi.org/10.1016/j.jclepro.2016.05.147.
[3] D. Liu, X. Min, Y. Ke, L. Chai, Y. Liang, Y. Li, L. Yao, Z. Wang, Co-treatment of flotation waste, neutralization sludge, and arsenic-containing gypsum sludge from copper smelting: solidification/stabilization of arsenic and heavy metals with minimal cement clinker, Environ. Sci. Pollut. Res. 25 (8) (2018) 7600–7607, https://doi.org/10.1007/s11356-017-1084-x.
[4] Y. Li, X. Min, L. Chai, M. Shi, C. Tang, Q. Wang, Y. Liang, J. Lei, W. Liyang, Co-treatment of gypsum sludge and Pb/Zn smelting slag for the solidification of sludge containing arsenic and heavy metals, J. Environ. Manag. 181 (2016) 756–761, https://doi.org/10.1016/j.jenvman.2016.07.031.
[5] J. Fei, T. Wang, Y. Zhou, Z. Wang, X. Min, Y. Ke, W. Hu, L. Chai, Aromatic organoarsenic compounds (AOCs) occurrence and remediation methods, Chemosphere 207 (2018) 665–675, https://doi.org/10.1016/j.chemosphere.2018.05.145.
[6] M.E. LeBlanc, M.B. Parsons, E.E.V. Chapman, L.M. Campbell, Review of ecological mercury and arsenic bioaccumulation within historical gold mining districts of Nova Scotia, Environ. Rev. 28 (2) (2020) 187–198, https://doi.org/10.1139/er-2019-0042.
[7] R. Hamberg, C. Maurice, L. Alakangas, Lowering the water saturation level in cemented paste backfill mixtures – Effect on the release of arsenic, Miner. Eng. 112 (2017) 84–91, https://doi.org/10.1016/j.mineng.2017.05.005.
[8] F.R. Costa, G.P. Nery, C.D. Carneiro, H. Kahn, C. Ulsen, Mineral characterization of low-grade gold ore to support geometallurgy, J. Mater. Res. Technol. Jmrt. 21 (2022) 2841–2852, https://doi.org/10.1016/j.jmrt.2022.10.085.
[9] Y. Wang, X. Fang, P. Deng, Z.H. Rong, X.C. Tang, S. Cao, Study on thermodynamic model of arsenic removal from oxidative acid leaching, J. Mater. Res. Technol. Jmrt. 9 (3) (2020) 3208–3218, https://doi.org/10.1016/j.jmrt.2020.01.068.
[10] C. Vandecasteele, V. Dutré, D. Geysen, G. Wauters, Solidification/stabilisation of arsenic bearing fly ash from the metallurgical industry. Immobilisation mechanism of arsenic, Waste Manag. 22 (2) (2002) 143–146, https://doi.org/10.1016/S0956-053X(01)00062-9.
[11] A.J. Bull, M. Fall, Curing temperature dependency of the release of arsenic from cemented paste backfill made with Portland cement, J. Environ. Manag. 269 (2020) 110772, https://doi.org/10.1016/j.jenvman.2020.110772.
[12] J.C. Ng, J. Wang, A. Shraim, A global health problem caused by arsenic from natural sources, Chemosphere 52 (9) (2003) 1353–1359, https://doi.org/10.1016/S0045-6535(03)00470-3.
[13] C.E. Tommaseo, M. Kersten, Aqueous solubility diagrams for cementitious waste stabilization systems. 3. Mechanism of zinc immobilizaton by calcium silicate hydrate, Environ. Sci. Technol. 36 (13) (2002) 2919–2925, https://doi.org/10.1021/es0102484.
[14] B.Y. Li, J.X. Zhang, H. Yan, N. Zhou, M. Li, Experimental investigation into the thermal conductivity of gangue-cemented paste backfill in mine application, J. Mater. Res. Technol. Jmrt. 16 (2022) 1792–1802, https://doi.org/10.1016/j.jmrt.2021.12.123.
[15] G.J. Wang, Q. Sun, C.X. Qi, L. Liu, Y. Tan, L.J. Su, Mechanical properties and microscopic characterization of cemented paste backfill with electrolytic manganese residue matrix binder, J. Mater. Res. Technol. -Jmrt. 23 (2023) 2075–2088, https://doi.org/10.1016/j.jmrt.2023.01.098.
[16] Y. Zhang, W. Gao, W. Ni, S. Zhang, Y. Li, K. Wang, X. Huang, P. Fu, W. Hu, Influence of calcium hydroxide addition on arsenic leaching and solidification/stabilisation behaviour of metallurgical-slag-based green mining fill, J. Hazard. Mater. 390 (2020) 122161, https://doi.org/10.1016/j.jhazmat.2020.122161.
[17] C. Zhang, J. Wang, W.D. Song, J.X. Fu, Pore structure, mechanical behavior and damage evolution of cemented paste backfill, J. Mater. Res. Technol. Jmrt. 17 (2022) 2864–2874, https://doi.org/10.1016/j.jmrt.2022.02.010.
[18] M. Sari, E. Yilmaz, T. Kasap, Long-term ageing characteristics of cemented paste backfill: usability of sand as a partial substitute of hazardous tailings, J. Clean. Prod. 401 (2023) 136723, https://doi.org/10.1016/j.jclepro.2023.136723.
[19] Q.S. Chen, K. Luo, Y.M. Wang, X.S. Li, Q.L. Zhang, Y.K. Liu, In-situ stabilization/solidification of lead/zinc mine tailings by cemented paste backfill modified with low-carbon bentonite alternative, J. Mater. Res. Technol. Jmrt. 17 (2022) 1200–1210, https://doi.org/10.1016/j.jmrt.2022.01.099.
[20] J. Li, S. Cao, E. Yilmaz, Analyzing the microstructure of cemented fills adding polypropylene-glass fibers with X-ray micro-computed tomography, J. Mater. Res. Technol. 27 (2023) 2627–2640, https://doi.org/10.1016/j.jmrt.2023.10.104.
[21] M. Sari, E. Yilmaz, T. Kasap, S. Karasu, Exploring the link between ultrasonic and strength behavior of cementitious mine backfill by considering pore structure, Constr. Build. Mater. 370 (2023) 130588, https://doi.org/10.1016/j.conbuildmat.2023.130588.
[22] Q. Sun, S. Tian, Q. Sun, B. Li, C. Cai, Y. Xia, X. Wei, Q. Mu, Preparation and microstructure of fly ash geopolymer paste backfill material, J. Clean. Prod. 225 (2019) 376–390, https://doi.org/10.1016/j.jclepro.2019.03.310.
[23] A.J. Bull, M. Fall, Thermally induced changes in metalloid leachability of cemented paste backfill that contains blast furnace slag, Miner. Eng. 156 (2020) 106520, https://doi.org/10.1016/j.mineng.2020.106520.
[24] S. Coussy, M. Benzaazoua, D. Blanc, P. Moszkowicz, B. Bussière, Arsenic stability in arsenopyrite-rich cemented paste backfills: A leaching test-based assessment, J. Hazard. Mater. 185 (2-3) (2011) 1467–1476, https://doi.org/10.1016/j.jhazmat.2010.10.070.
[25] J.V. Bothe, P.W. Brown, Arsenic immobilization by calcium arsenate formation, Environ. Sci. Technol. 33 (21) (1999) 3806–3811, https://doi.org/10.1021/es980998m.
[26] J. Camacho, H. Wee, T.A. Kramer, R. Autenrieth, Arsenic stabilization on water treatment residuals by calcium addition, J. Hazard. Mater. 165 (1-3) (2009) 599–603, https://doi.org/10.1016/j.jhazmat.2008.10.038.
[27] H.W. Godbee, E.L. Compere, D.S. Joy, A.H. Kibbey, R. Neilsonjr, Application of mass transport theory to the leaching of radionuclides from waste solid, Nucl. Chem. Waste Manag. 1 (1) (1980) 29–35, https://doi.org/10.1016/0191-815X(80)90026-1.
[28] M. Chrysochoou, D. Dermatas, Evaluation of ettringite and hydrocalumite formation for heavy metal immobilization: Literature review and experimental study, J. Hazard. Mater. 136 (1) (2006) 20–33, https://doi.org/10.1016/j.jhazmat.2005.11.008.
[29] D.H. Moon, D. Dermatas, N. Menounou, Arsenic immobilization by calcium-arsenic precipitates in lime treated soils, Sci. Total Environ. 330 (1-3) (2004) 171–185, https://doi.org/10.1016/j.scitotenv.2004.03.016.
[30] A.B. Ghazi, A. Jamshidi-Zanjani, H. Nejati, Clinkerisation of copper tailings to replace Portland cement in concrete construction, J. Build. Eng. 51 (2022) 104275, https://doi.org/10.1016/j.jobe.2022.104275.
[31] A. Saedi, A. Jamshidi-Zanjani, M. Mohseni, A.K. Darban, Mechanical activation for sulfidic tailings treatment by tailings: Environmental aspects and cement consumption reduction, Case Stud. Constr. Mater. 19 (2023), https://doi.org/10.1016/j.cscm.2023.e02632.
[32] H. Jiang, J. Han, Y. Li, E. Yilmaz, Q. Sun, J. Liu, Relationship between ultrasonic pulse velocity and uniaxial compressive strength for cemented paste backfill with alkali-activated slag, Nondestruct. Test. Eval. 35 (4) (2020) 359–377, https://doi.org/10.1080/10589759.2019.1679140.
[33] N. Ouffa, R. Trauchessec, M. Benzaazoua, A. Lecomte, T. Belem, A methodological approach applied to elaborate alkali-activated binders for mine paste backfills, Cem. Concr. Compos. 127 (2022) 104381, https://doi.org/10.1016/j.cemconcomp.2021.104381.

[34] S. Zhang, F. Ren, Y. Zhao, J. Qiu, Z. Guo, The effect of stone waste on the properties of cemented paste backfill using alkali-activated slag as binder, Constr. Build. Mater. 283 (2021) 122686, https://doi.org/10.1016/j.conbuildmat.2021.122686.
[35] F. Cihangir, Y. Akyol, Effect of desliming of tailings on the fresh and hardened properties of paste backfill made from alkali-activated slag, Adv. Mater. Sci. Eng. 2020 (2020) 1–11, https://doi.org/10.1155/2020/4536257.
[36] H. Jiang, L. Ren, X. Gu, J. Zheng, L. Cui, Synergistic effect of activator nature and curing temperature on time-dependent rheological behavior of cemented paste backfill containing alkali-activated slag, Environ. Sci. Pollut. Res. 30 (5) (2023) 12857–12871, https://doi.org/10.1007/s11356-022-23053-1.
[37] Y. Kou, H. Jiang, L. Ren, E. Yilmaz, Y. Li, Rheological properties of cemented paste backfill with alkali-activated slag, Minerals 10 (3) (2020) 288, https://doi.org/10.3390/min10030288.
[38] W. Qi, Q. Ren, Q. Zhao, Y. Feng, W. Qi, Y. Han, Y. Huang, Effectiveness of soda residue-activated GGBS as alternative binder on compressive strength and workability of cemented paste backfills: reuse of multi-source solid wastes, Constr. Build. Mater. 348 (2022) 128594, https://doi.org/10.1016/j.conbuildmat.2022.128594.
[39] G. Zhu, W. Zhu, Y. Fu, B. Yan, H. Jiang, Effects of chloride salts on strength, hydration, and microstructure of cemented tailings backfill with one-part alkali-activated slag, Constr. Build. Mater. 374 (2023) 130965, https://doi.org/10.1016/j.conbuildmat.2023.130965.
[40] H.Q. Jiang, Z.J. Qi, E. Yilmaz, J. Han, J.P. Qiu, C.L. Dong, Effectiveness of alkali-activated slag as alternative binder on workability and early age compressive strength of cemented paste backfills, Constr. Build. Mater. 218 (2019) 689–700, https://doi.org/10.1016/j.conbuildmat.2019.05.162.
[41] H. Jiang, Z. Qi, E. Yilmaz, J. Han, J. Qiu, C. Dong, Effectiveness of alkali-activated slag as alternative binder on workability and early age compressive strength of cemented paste backfills, Constr. Build. Mater. 218 (2019) 689–700, https://doi.org/10.1016/j.conbuildmat.2019.05.162.
[42] F. Cihangir, B. Ercikdi, A. Kesimal, H. Deveci, F. Erdemir, Paste backfill of high-sulphide mill tailings using alkali-activated blast furnace slag: effect of activator nature, concentration and slag properties, Miner. Eng. 83 (2015) 117–127, https://doi.org/10.1016/j.mineng.2015.08.022.
[43] A.A. Aliabdo, A.E.M. Abd Elmoaty, M.A. Emam, Factors affecting the mechanical properties of alkali activated ground granulated blast furnace slag concrete, Constr. Build. Mater. 197 (2019) 339–355, https://doi.org/10.1016/j.conbuildmat.2018.11.086.
[44] A. Fernández-Jiménez, J.G. Palomo, F. Puertas, Alkali-activated slag mortars: mechanical strength behaviour, Cem. Concr. Res. 29 (8) (1999) 1313–1321, https://doi.org/10.1016/S0008-8846(99)00154-4.
[45] S.D. Wang, K.L. Scrivener, P.L. Pratt, Factors affecting the strength of alkali-activated slag, Cem. Concr. Res. 24 (6) (1994) 1033–1043, https://doi.org/10.1016/0008-8846(94)90026-4.
[46] M.D. Andersen, H.J. Jakobsen, J. Skibsted, Incorporation of aluminum in the calcium silicate hydrate (C-S-H) of hydrated portland cements: a high-field 27Al and 29Si MAS NMR investigation, Inorg. Chem. 42 (7) (2003) 2280–2287, https://doi.org/10.1021/ic020607b.
[47] F. Puertas, M. Palacios, H. Manzano, J.S. Dolado, A. Rico, J. Rodríguez, A model for the C-A-S-H gel formed in alkali-activated slag cements, J. Eur. Ceram. Soc. 31 (12) (2011) 2043–2056, https://doi.org/10.1016/j.jeurceramsoc.2011.04.036.
[48] I.G. Richardson, A.R. Brough, R. Brydson, G.W. Groves, C.M. Dobson, Location of aluminum in substituted calcium silicate hydrate (C-S-H) gels as determined by 29Si and 27Al NMR and EELS, J. Am. Ceram. Soc. 76 (9) (2010), https://doi.org/10.1111/j.1151-2916.1993.tb07765.x.
[49] S. Song, H.M. Jennings, Pore solution chemistry of alkali-activated ground granulated blast-furnace slag11This paper was originally submitted to Advanced Cement Based Materials. The paper was received at the Editorial Office of Cement and Concrete Research on 12 November 1998 and accepted in final form on 16 November 1998, Cem. Concr. Res. 29 (2) (1999) 159–170, https://doi.org/10.1016/S0008-8846(98)00212-9.
[50] W. Zhang, D. Hou, P. Wang, J. Xu, Z. Li, Mesoscale simulation of the effect of pH on the hydration rate, morphology, and mechanical performance of a calcium-silicate-hydrate gel, J. Mater. Civ. Eng. 35 (9) (2023) 4023302, https://doi.org/10.1061/JMCEE7.MTENG-15044.
[51] K. Suzuki, T. Nishikawa, S. Ito, Formation and carbonation of C-S-H in water, Cem. Concr. Res. 15 (2) (1985) 213–224, https://doi.org/10.1016/0008-8846(85)90032-8.
[52] K. Suzuki, T. Nishikawa, H. Ikenaga, S. Ito, Effect of NaCl or NaOH on the formation of C S H, Cem. Concr. Res. 16 (3) (1986) 333–340, https://doi.org/10.1016/0008-8846(86)90108-0.
[53] A. Saedi, A. Jamshidi-Zanjani, A.K. Darban, M. Mohseni, H. Nejati, Utilization of lead–zinc mine tailings as cement substitutes in concrete construction: effect of sulfide content, J. Build. Eng. 57 (2022) 104865, https://doi.org/10.1016/j.jobe.2022.104865.
[54] B. Guo, B. Liu, J. Yang, S. Zhang, The mechanisms of heavy metal immobilization by cementitious material treatments and thermal treatments: a review, J. Environ. Manag. 193 (2017) 410–422, https://doi.org/10.1016/j.jenvman.2017.02.026.
[55] R.B. Perkins, C.D. Palmer, Solubility of chromate hydrocalumite (3CaO·Al2O3·CaCrO4·nH2O) 5–75°C 31 (7) (2001) 983–992, https://doi.org/10.1016/S0008-8846(01)00507-5.
[56] S. Ahmari, L. Zhang, J. Zhang, Effects of activator type/concentration and curing temperature on alkali-activated binder based on copper mine tailings, J. Mater. Sci. 47 (16) (2012) 5933–5945, https://doi.org/10.1007/s10853-012-6497-9.
[57] M. Ben Haha, G. Le Saout, F. Winnefeld, B. Lothenbach, Influence of activator type on hydration kinetics, hydrate assemblage and microstructural development of alkali activated blast-furnace slags, Cem. Concr. Res. 41 (3) (2011) 301–310, https://doi.org/10.1016/j.cemconres.2010.11.016.
[58] E. Deir, B.S. Gebregziabiher, S. Peethamparan, Influence of starting material on the early age hydration kinetics, microstructure and composition of binding gel in alkali activated binder systems, Cem. Concr. Compos. 48 (2014) 108–117, https://doi.org/10.1016/j.cemconcomp.2013.11.010.
[59] I. Garcia-Lodeiro, A. Palomo, A. Fernández-Jiménez, D.E. Macphee, Compatibility studies between N-A-S-H and C-A-S-H gels. Study in the ternary diagram Na2O–CaO–Al2O3–SiO2–H2O, Cem. Concr. Res. 41 (9) (2011) 923–931, https://doi.org/10.1016/j.cemconres.2011.05.006.
[60] S. Hong, F.P. Glasser, Alkali sorption by C-S-H and C-A-S-H gels: Part II. Role of alumina, Cem. Concr. Res. 32 (7) (2002) 1101–1111, https://doi.org/10.1016/S0008-8846(02)00753-6.
[61] S. Yoshida, Y. Elakneswaran, T. Nawa, Electrostatic properties of C–S–H and C-A-S-H for predicting calcium and chloride adsorption, Cem. Concr. Compos. 121 (2021) 104109, https://doi.org/10.1016/j.cemconcomp.2021.104109.
[62] E. Altan, S.T. Erdoğan, Alkali activation of a slag at ambient and elevated temperatures, Cem. Concr. Compos. 34 (2) (2012) 131–139, https://doi.org/10.1016/j.cemconcomp.2011.08.003.
[63] H. Jiang, L. Ren, Q. Zhang, J. Zheng, L. Cui, Strength and microstructural evolution of alkali-activated slag-based cemented paste backfill: coupled effects of activator composition and temperature, Powder Technol. 401 (2022) 117322, https://doi.org/10.1016/j.powtec.2022.117322.
[64] V. Živica, Effects of type and dosage of alkaline activator and temperature on the properties of alkali-activated slag mixtures, Constr. Build. Mater. 21 (7) (2007) 1463–1469, https://doi.org/10.1016/j.conbuildmat.2006.07.002.
[65] M. Fall, J.C. Célestin, M. Pokharel, M. Touré, A contribution to understanding the effects of curing temperature on the mechanical properties of mine cemented tailings backfill, Eng. Geol. 114 (3-4) (2010) 397–413, https://doi.org/10.1016/j.enggeo.2010.05.016.
[66] H. Jiang, H. Yi, E. Yilmaz, S. Liu, J. Qiu, Ultrasonic evaluation of strength properties of cemented paste backfill: effects of mineral admixture and curing temperature, Ultrasonics 100 (2020) 105983, https://doi.org/10.1016/j.ultras.2019.105983.